Journal of Manufacturing Processes 38 (2019) 387–395

Contents lists available at ScienceDirect

Journal of Manufacturing Processes

journal homepage: www.elsevier.com/locate/manpro

Mechanical, thermal and micrographic investigations of friction stir welded: 3D printed melt flow compatible dissimilar thermoplastics

Ranvijay Kumar[a,b], Rupinder Singh[a,*], I.P.S. Ahuja[b]

[a] Dept. of Production Engineering, Guru Nanak Dev Engineering College, Ludhiana, India
[b] Dept. of Mech. Engineering, Punjabi University, Patiala, India

ARTICLE INFO

Keywords:
FSW
MFI
Thermal imaging
Al reinforcement
ABS
PA6

ABSTRACT

In this study, effort has been made to prepare aluminium (Al) reinforced thermoplastic composites of acrylonitrile butadiene styrene (ABS) and polyamide6 (PA6) with twin screw extrusion (TSE) followed by 3D printing of functional prototype on fused deposition modelling (FDM) setup for exploring the possibilities of joining with controlled melt flow properties. The 3D printed Al reinforced ABS and PA6 thermoplastic composite based functional prototypes were welded with friction stir welding (FSW) on vertical milling. The joints were subjected to tensile, flexural, thermal and photo-micrographic investigations. It has been observed that reinforcement of 15% Al to ABS matrix and 50% Al to PA6 matrix resulted into similar melt flow index (MFI) and maximum tensile, flexural properties were obtained at 1400 rpm, 30 mm/min feed rate and 4 mm plunge depth with minimum force 52 N (in the present case study). These results will be helpful for joining/crack filling of oil/gas pipeline with significantly reduced downtime.

1. Introduction

There is promising requirement of compatibility, light weight, stronger, flexible and low cost materials in many industrial/engineering prospective [1]. Thermoplastic composite is one of the best alternatives with prospects of low cost and tailorabilty in various engineering applications [2]. FSW is a meticulously developed joining technique which joins two materials in solid state phase, having advantages over conventional welding techniques such as; less defects, less power requirements, no use of consumables and highly characterized weld qualities etc. [3,4]. The FSW machine tool are generally configured with a set of clamping mechanism, tool holder, pin and shoulder arrangements and external accessories for forces, temperature and flow measurements. The basic functionality of tool-shoulder arrangement is to critically control the material flow and localized heating at the interface of structures to ascertain the microstructures and mechanical strengths [5]. It was observed that weld quality is the key function of tool geometries and input process variable, as study suggested that torque in FSW is dependent of tool geometry, welding speed and tool rotation speed [6]. The FSW conducted for Al-magnesium (Mg) alloy and polycarbonate (PC) has revealed the interesting facts that at optimum rotational speed (1600 rpm) and transverse speed (45 mm/min), the hardness of PC weld zone was reduced due to reduction in molecular weight as well as micro-hardness of Al-Mg weld zone was increased due to grain refinement [7]. For superior surface and weld strength quality, the stationary shoulder of Teflon polymeric materials with certain grooves has been resulted better as compare to Al, brass and wooden shoulders [8]. The mechanical properties for joint of HDPE-carbon black composite is an output of welding speed and pin depth penetration [9]. It has been reported that reducing welding speed from 30 mm/min to 20 mm/min and plunge depth form 4.2 mm to 4.1 mm resulted into loss of yield strength up to 37% and yield strain up to 74% to the parent material. The FSW of two similar thermoplastic materials is an easy approach for producing butt joints and various studies have been reported with different edge of tooling consideration, but FSW of dissimilar thermoplastic is a difficult process because every thermoplastic have their own molecular weight, melt flow index (MFI), viscosity, melting point, glass transition temperature, and carbon chain arrangement [10–13]. The compatibility between welding specimens is the major issue which restricts the joining efficiency better joining strength. The study reported to address that issue is to make selected thermoplastics (e.g ABS and PA6) by use of metal particle is significantly acceptable technique with help of melt processing techniques (e.g. 3D printing and extrusion) [14]. The use of nano or micro sized particle into thermoplastic matrix is a smart technique which ensure the better material flow and heat formation during stirring, It was reported that addition of nano-silica for ABS joining improved the welding strength by 26% [15]. Since heat generation is the key factor of the FSW

* Corresponding author.
E-mail addresses: ranvijayk12@gmail.com (R. Kumar), rupindersingh78@yahoo.com (R. Singh), Ahujaahujaips@gmail.com (I.P.S. Ahuja).

https://doi.org/10.1016/j.jmapro.2019.01.043
Received 3 November 2018; Received in revised form 9 January 2019; Accepted 22 January 2019

process for joining of dissimilar materials, a study was conducted for joining of Al alloy (Al6082-T6) to self reinforced polypropylene (PP) sheets and it was suggested a technique that making pre-holes in Al6082-T6 sheet can support the back extrusion (with concentrated heat generation) of thermoplastic PP, which provided feasibility of metal alloy to thermoplastic joining [16]. The FSW of dissimilar thermoplastics in some situation is infeasible because of lack of heat formation, inferior fusion which creates large voids and improper tool design. A study reported that an assisted arrangement of heating tool in FSW setup improved the ductility of the PP joints [17]. For FSW of dissimilar material, Formation of inter-metallic compound is a serious problem which minimizes the strength of the joints; the extrusion based joining called friction stir extrusion (FSE) can be helpful to minimize the chances of formation of inter-metallic compounds, the process can also be applicable to wide range of thermoplastic [18]. The strength of the dissimilar joints (like Al alloy to polymer) is dependent upon mechanical interlocking and adhesive bonding, which can be enhanced by optimizing welding speed and tool geometry [19]. It is also reported that pre-heating is helpful for grain refinement by friction stir processing (FSP) and can be further subject to FSW for dissimilar thermoplastic materials [20]. Observations have been made regarding FSW of AA2060-T8 and short carbon fiber reinforced polyether ether ketone (PEEK) that combination of stationary shoulder and tapered thread pin with the triple facets resulted better joints performances [21]. With minor modification in the machine, tool or the material processing, a wide range of materials can be prepared for variety of purposes [22]. Some studies of technological feasibility, material flow behavior during FSW process, compatibility issues of dissimilar thermoplastics, and investigations of weld quality by input process variables have been reported in recent past [21,22]. These studies have found interesting aspects of optimizing tool and process, focusing the fusion improvement, improving heat generations by means of tool design and particle reinforcement [5,8,12,11–13,15,22]. Overall a gap with issues in material compatibility has been observed while FSW of thermoplastics, which may be covered by understanding material deformation mechanism and controlling the processing variables. The ABS thermoplastic has wide range of applications (such as material prototypes, construction, pipe and fitting, vacuum construction as sustainable structures). The PA6 is semi crystalline thermoplastic which has high elastic modulus, elongation properties and thermal, chemical and wears resistive characteristics (which covers almost all engineering fields). Since there is a large gap of basic properties (physical/ mechanical/ thermal/ rheological etc.) of ABS and PA6, so these two thermoplastics may be classified as of dissimilar category. In the present work detailed methodology for joining of dissimilar thermoplastics with friction stir welding has been outlined as a case study of ABS and PA6. There are number of reasons for selecting the Al metal particle for reinforcement over other metals particles:

- high thermal conductivity (almost twice of copper)
- good reflector of visible lights
- highly corrosive resistance to restrict the formation of oxides
- high ductility, low melting points and light weights.
- Also the friction stir welding of Al and its alloys is established process.
- However other low melting alloys such as Cu, brass etc. may be explored for further studies both for friction as well as friction stir welding.

The present study addresses the processing of compatible dissimilar plastic based materials (Al reinforced ABS and PA6) for FSW process. For this study, reinforcement of 15%Al to ABS matrix (by weight) and reinforcement of 50% Al to PA matrix resulted in almost similar MFI of 11.57 g/10 min (for ABS-15%Al) and 11.97 g/10 min (for PA-50%Al).

2. Materials and methods

The primary recycled commercial grade of ABS (Grade- EX58) and PA6 (Grade- P X 99,848) were procured from local market (Batra Polymers Pvt Ltd, Ludhiana, India). Initially without investigating the basic properties, sheets of ABS and PA6 were fabricated by extrusion and 3D printing on fixed process variables. The prepared parts were clamped to FSW setup (vertical milling machine configured with dynamometer and thermal imaging) and welding was processed. The joints were unable to form and welding of these two virgin thermoplastic were failed. It was observed during FSW process that ABS was melted first and at the same time there was no melting for PA6. Those observations have found in the form that there should be the melting temperature and melt flow gap between ABS and PA6.

The melting point of these thermoplastics have been investigated by differential scanning calorimetric (DSC) setup (Company: Mettler Toledo, Model:DSC822e) and found 190.00–193.49 °C for ABS and 223.29 °C for PA6. The MFI (MFI setup: Shanta engineering, Pune, India, Model: 2013) of virgin ABS and PA6 was 8.76 g/10 min, 23.27 g/10 min respectively (calculated as per ASTM D1238). The MFI of these two thermoplastic have been modified by Al metal particle reinforcement (50 μm particle sized procured from Shiva Chemical Pvt Ltd., Ludhiana, India) for welding compatibility. Again the MFI of reinforced Al metal particle to ABS and PA6 thermoplastic have been investigated in different weight proportions from 5 to 50% (see Table 1). The results of MFI indicated that ABS with 15% Al content and PA6 with 50% Al content were similar (11.57 g/10 min and 11.97 g/10 min). So, for further experimentation, ABS-15%Al and PA6-50%Al were judicially selected.

The selected composition of ABS-15%Al and PA6-50%Al were processed with TSE (Company: Themo scientific, Model: HAAKE MiniCTW) for feedstock filament preparations. The ABS-15%Al was processed at 220 °C barrel temperature, 30 rpm screw speed and with 20Kg external

Table 1
MFI of virgin ABS, PA6, and Al reinforced ABS and PA6 [23].

Material Composition	MFI (g/10 min)				Material Composition	MFI (g/10 min)			
	Trial 1	Trial 2	Trial 3	Avg.		Trial 1	Trial 2	Trial 3	Avg.
Virgin ABS	9.05	8.39	8.86	8.76	Virgin PA6	23.58	23.27	22.98	23.27
ABS + 5%Al	8.11	10.39	9.71	9.4	PA6 + 5%Al	25.17	23.01	25.4	24.52
ABS + 10% Al	10.54	10.57	9.27	10.12	PA6 + 10% Al	29.82	30.56	29.09	29.82
ABS + 15% Al	11.44	11.8	11.48	11.57	PA6 + 15% Al	33.05	30.93	30.89	31.62
ABS + 20% Al	12.47	12.49	12.98	12.64	PA6 + 20% Al	35.23	34.54	33.45	34.4
ABS + 25% Al	10.38	11.12	10.98	10.82	PA6 + 25% Al	38.87	33.64	35.53	36.01
ABS + 30% Al	10.26	10.59	10.01	10.28	PA6 + 30% Al	36.85	35.39	36.88	36.37
ABS + 35% Al	9.37	10.63	9.98	9.99	PA6 + 35% Al	31.82	29.86	28.54	30.07
ABS + 40% Al	9.33	8.87	9.23	9.14	PA6 + 40% Al	20.23	21.11	23.23	21.52
ABS + 45% Al	7.23	7.43	8.04	7.56	PA6 + 45% Al	15.02	19.27	16.94	17.07
ABS + 50% Al	7.09	6.81	5.56	6.48	PA6 + 50% Al	10.76	12.33	12.84	11.97

Table 2
Mechanical, thermal and morphological properties of 3D printed ABS-15%Al and PA6-50%Al [14,24].

Materials	ABS-15%Al	PA6-50%Al
Peak Load (N)	655.87	660.12
Break Load (N)	652.54	655.37
Elongation at peak (mm)	5.62	7.24
Elongation at break (mm)	8.45	12.5
MFI (g/10 min)	11.57	11.97
Porosity (%)	11.17	31.71
Melting point (°C)	203.20-223.59	221.06

load, whereas PA6-50%Al was processed at 245 °C, 20 rpm screw speed and with 15Kg external load (based upon uniformity of feedstock filaments). The commercial fused deposition modeling (FDM), (Company: Divide by Zero, India, Model: Accucraft 250D) setup was used at following fixed parameteric settings:

infill percentage of 80%, filament diameter of 1.75 ± 0.05 mm, 6 number of perimeters, rectilinear filling, perimeter speed of 30 mm/sec, printing speed 60 mm/sec, extruder temperature of 250 °C and printing bed temperature at 55 °C.

The mechanical (on universal tensile tester, Company: Shanta Engineering, India, Model: SE-500Kgf), thermal and morphological (by optical microscope, Model: XJL-17) properties of FDM printed ABS-15%Al and PA6-50%Al parts have been checked as shown in Table 2. ASTM D638 type IV (speed: 50/min) was followed for tensile properties evaluation and ASTM D 790 for flexural properties. ASTM E0794-01 for DSC analysis and ASTM E2015-04(2014) were followed for morphological properties.

3. Experimentations

On fixed input setting, ABS-15%Al and PA6-50%Al sheets with dimension of 60 × 60 × 4 mm were printed on FDM setup for FSW on vertical milling setup. Fig. 1 Shows 3D printed melt flow compatible welding specimens of Al reinforced thermoplastics.

For experimentation of FSW on vertical milling setup, there are 3 input process variable have been selected (namely: rotational speed, traverse speed and plunge depth). During pilot experimentation of FSW, it was observed that between rotational speeds of 800–1600 rpm, traverse speed of 30–60 mm/min and plunge depth 2–4 mm, the weld formation appeared as defect less. So, based upon the trial experiments, the level of input variables have been selected as shown in Table 3. The design of experimental for present study is based upon the well established Taguchi L9 orthogonal array. The Taguchi L9 orthogonal itself reduces the 27 set of experiment to 9 set of experiment.

Table 3
Design of experimentation with levels of input process variables.

Experiment no.	Rotational Speed (rpm)	Traverse speed (mm/min)	Plunge depth (mm)
1	1000	30	2
2	1000	40	3
3	1000	50	4
4	1200	30	3
5	1200	40	4
6	1200	50	2
7	1400	30	4
8	1400	40	2
9	1400	50	3

Fig. 2 (a) show the FSW setup, configured with thermal imaging camera and dynamometer. Fig. and Fig. 2(b) shows actual experimental setup for present study equipped with milling dynamometer and thermal imaging camera. The thermal camera was held at angle of 30° and 0.5 m separation.

The conventional vertical milling setup has been configured with some measuring instrument for online monitoring of the weld. The thermal imaging camera (Manufacturer: Flir, Model: TG165) was attached with the vertical milling setup for measuring online temperature at the interface whereas dynamometer (Company: Industrial engineering instrument, India, Model: Multi-component digital force indicator, Model: 652) was used for investigating the requirement of forces at different input process variables. Fig. 3 shows the FSW welded melt flow compatible 3D printed structures. Based upon set of experimental conditions (see Table 3), welded joints prepared were further subjected to investigations of mechanical, thermal, morphological properties. The tensile properties of joints were observed by testing through ASTM 638 type IV standard whereas flexural properties by ASTM D790. The tensile and flexural testing results were consisted of peak load, break load, deflection at peak, and deflection at break. The downward forces acted by tool on specimen were measured by use of dynamometer and at the same time the thermal imaging camera was used to observe the changes in the interface temperature between joints. Thermal properties were subjected to observe the melting point and heat capacities by taking proportions (in mg) from joint interfaces. The thermal testing was conducted by two continuous heating between 30–250 °C (endothermic reaction) and cooling between 250-30 °C (exothermic reaction). Additionally, the percentage porosity at joint has been interpreted by using metallurgical image analysis software (MIAS) on optical microscope under 100X magnification.

Fig. 1. 3D printed melt flow compatible Al reinforced ABS and PA6 specimen for welding.

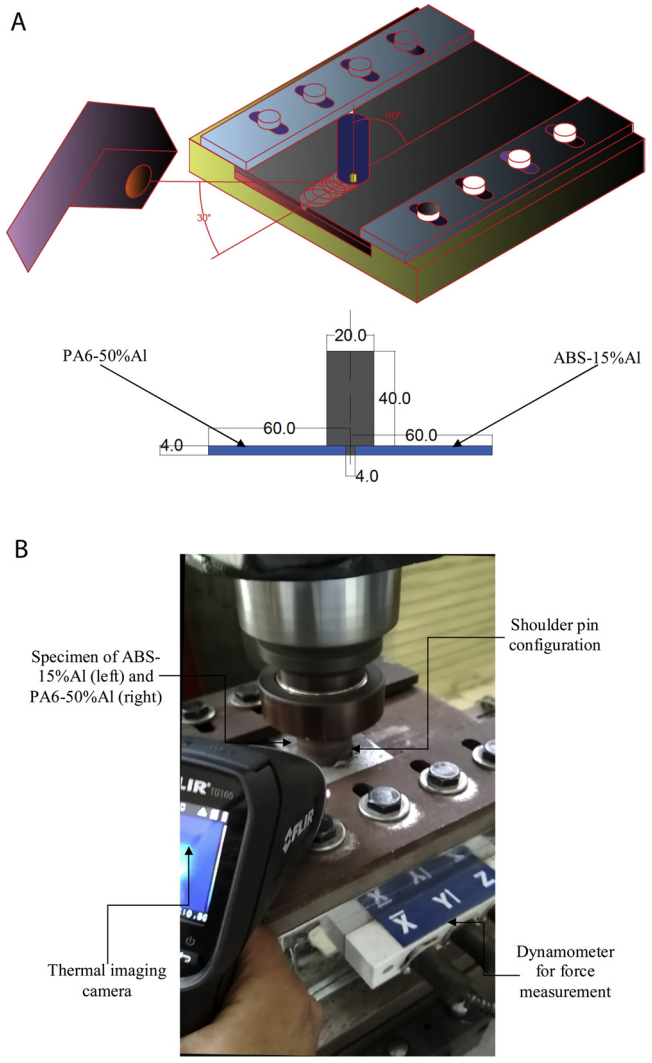

Fig. 2. (a) Schematic details of FSW process. (b) Experimental setup for FSW process.

4. Results and discussion

Critical and systematic examinations of failure mechanics, thermographs, morphology, and forces have been conducted to study the capabilities of joints produced by FSW. Under mechanics of joints, tensile (peak load, break load, elongation at peak, elongation at break) and flexural (peak load, break load, deflection at peak, and deflection at break) properties have been investigated at all 9 different set of experimentation. The morphology of the joints has been analyzed by exposing stirred zone on optical microscope integrated with MIAS analysis software. The online monitoring includes measurements of maximum axial force along with interface temperature of the joints during stirring process. Table 4 shows, mechanical, thermal, force and morphological properties of joints produced by FSW.

4.1. Mechanical properties

Based upon Table 4, the tensile and flexural properties have been presented in the form of stress vs, strain curves so that mechanics of ultimate failure can be observed. Fig. 4 shows stress vs, strain curves for tensile tested joints at all 9 different set of experiment. It should be noted that maximum tensile properties was obtained in experiment no. 7 (input variable combination: 1400 rpm, 30 mm/min and 4 mm plunge depth) whereas minimum tensile properties was obtained in experiment no. 2 (input variable combinations: 1000 rpm, 40 mm/min and 3 mm plunge depth). Here it may be predicted that maintaining maximum range of rpm, minimum traverse speed and maximum tool plunge depth resulted in maximum tensile properties. The smooth stirred zone observed in experiment no. 7 has influenced to get maximum tensile strength and elongation properties.

For changes in the tensile properties, higher range (1400 rpm) of rotational speed and plunge depth (4 mm) having lower range of traverse speed (30 mm/min) contributed maximum. This may be due to a fact that higher range of rotational speed provided maximum heat generation and hence stirring was appeared to be smooth.

Similarly, the 3 point bending (flexural test) was performed on all joints. It has been observed that maximum flexural loading was possible for experiment no. 7 and minimum for experiment no. 2 (See Fig. 5). It should be noted that load resisting capacity in flexural was achieved maximum and minimum analogous to tensile testing but deflection was bit altered. The minimum deflection was exhibited by joint in experiment no. 2, but the maximum flexural strength was observed in experiment no. 3 which has input variable combinations of lowest rotational speed (1000 rpm), highest traverse speed (50 mm/min) and highest plunge depth (4 mm).

4.2. Interface temperature

Temperature at interface is an indicator of the quality of stirred zone, which can lead to predict axial force requirements during processing. Here it should be noted that ultimate quality and soundness of the weld is largely dependent upon the mechanism of material flow

Fig. 3. welded specimen of melt flow compatible ABS-15% Al and PA6-50%Al.

Table 4
Mechanical, thermal, force and morphological properties of joints produced by FSW.

Exp no.	Tensile properties				Flexural Properties				Maximum Axial Force (N)	Interface Temperature (°C)	Porosity at Joints (%)
	Peak Load (N)	Break Load (N)	Elongation at Peak (mm)	Elongation at Break (mm)	Peak Load (N)	Break Load (N)	Deflectionat Peak (mm)	Deflection at Break (mm)			
1	232.92	209.62	2.09	2.09	110.2	100.08	5.13	9.12	301	80.9	19.25
2	118.66	106.8	0.95	0.95	90.8	80.82	0.95	2.47	380	79.4	24.24
3	412.87	371.59	2.47	2.66	130.7	120.33	2.09	11.21	142	111.4	16.45
4	190.26	171.23	1.14	1.14	180.6	160.74	4.37	9.69	360	85.8	22.42
5	309.41	278.47	3.04	3.04	350.3	310.77	3.8	6.27	201	106.4	17.19
6	300.09	270.08	1.9	2.09	110.7	100.53	2.09	3.99	220	93.7	18.08
7	528.6	475.74	3.61	3.61	360.2	320.58	3.23	3.42	52	138.8	14.48
8	509.47	458.53	3.23	3.23	230.5	210.15	5.51	6.65	96	114.9	15.81
9	258.41	232.57	3.23	3.23	200.5	180.45	5.51	8.55	210	105.4	20.17

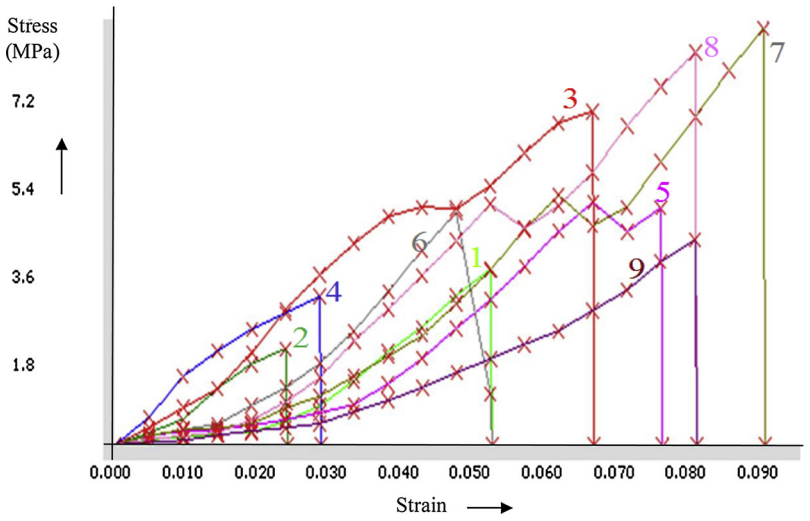

Fig. 4. Stress vs. strain curves for tensile properties.

during stirring. If the process variables are correct then there will be large amount of heat generation which can provide smooth stirred zone. The better heat generation efficiency means lower requirement of the axial force required during stirring and this will always lead to the better load resisting capacity of final joint produced. In the present case of FSW of 3D printed melt flow compatible ABS-%Al and PA-50%Al sheets, the maximum interface temperature was observed at experiment no. 7 (136.8 °C) whereas minimum interface temperature was observed at experiment no. 2 (79.4 °C) (see Fig. 6). It should be noted that at experiment no. 7, the requirement of the force was recorded minimum. So, here it is confirmed that giving high rotational speed with maintaining high plunge depth and low traverse speed can generate maximum heat due to which joints can sustain best as prospective of mechanical load capacities. Following the similar rule, the joints produced at experiment no. 2 was recorded with lowest temperature output (79.4 °C) due to which axial force requirement was maximum (380 N). The minimum heat generation at experiment no. 2 ensured the low mechanical sustainability of the joint.

It should be noted that establishing the emissivity value of thermal imaging camera is an important aspect because every material is having

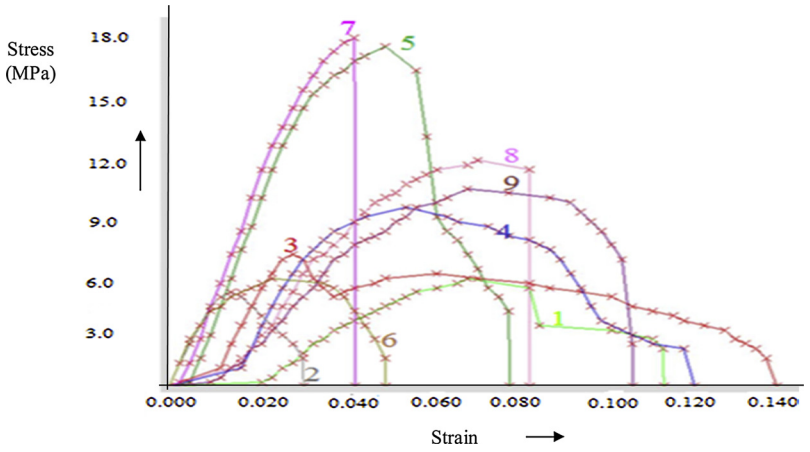

Fig. 5. Stress vs. strain curves for flexural properties.

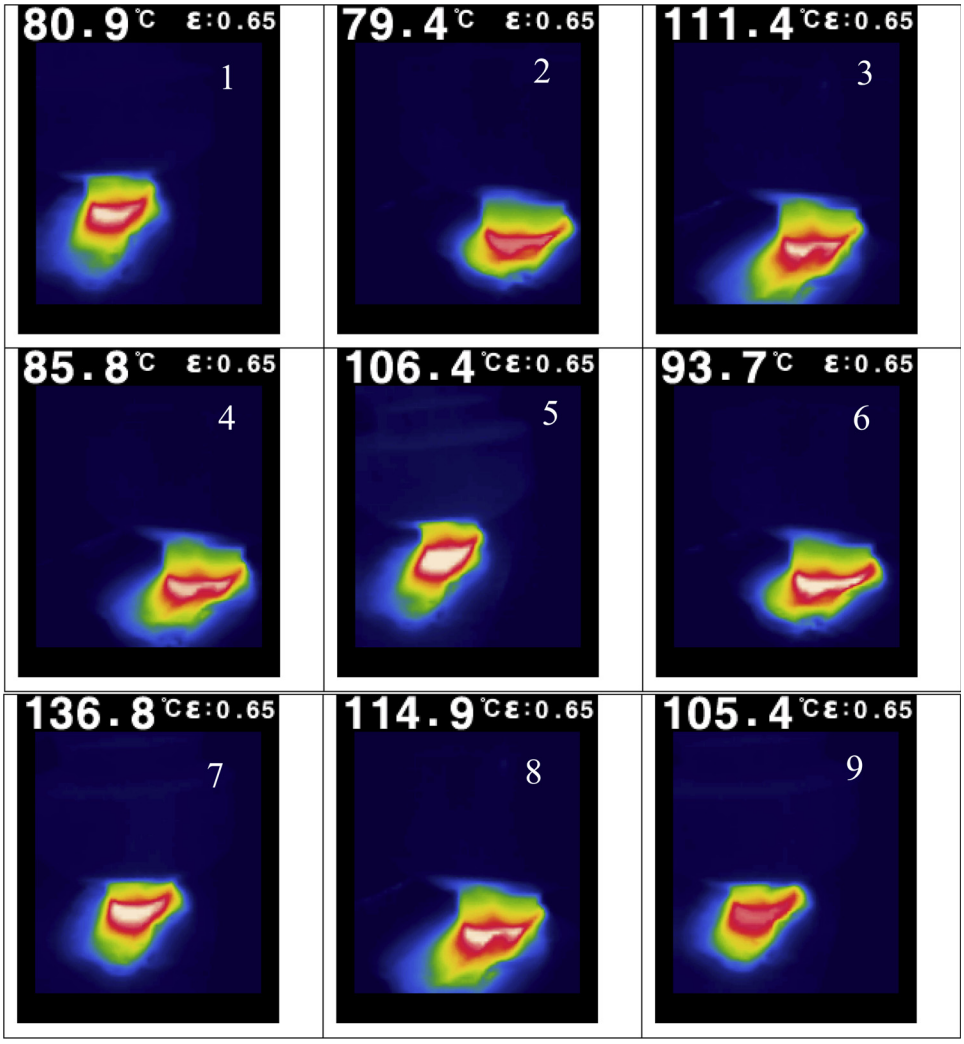

Fig. 6. Thermal imaging of joints during stirring process.

own emissivity [25–27]. It is reported that PA6 is having emissivity of 0.85 [28], ABS having 0.92 [29] and Al having 0.18 [30]. In the present study the FSW process is dealt with thermoplastics reinforced with different percentage. The ABS is reinforced with 50% Al and PA6 are reinforced with 50% Al. The given equations have been drawn as per composition;

(i)For ABS-15%Al (85%ABS and 15%Al), $0.85 \times 0.92 + 0.15 \times 0.18$. ..... (1)

(ii)For PA6-50%Al (50%PA6 and 50%Al), $0.50 \times 0.85 + 0.50 \times 0.18$ ..... (2)

Putting the values of emissivity in Eqs. (1) and (2) results emissivity of composites as;

ABS-15%Al 0 = 0.809 and PA6-50%Al = 0.515

The thermal imaging camera was focused on the interface of ABS-15%Al and PA6-50%Al sheets so that average of those have been fixed for experimentations as 0.662 (Approx. 0.65 in multiplier of 0.05).

4.3. Micrographs and macrographs

Micrographic observations made at 100X magnification results in an interesting fact that structures of the stirred surface were responsible for of mechanical loading capabilities and requirement of forces (see Fig. 7). Here it should be noted that in experiment no. 2 poor mechanical properties were obtained with maximum force requirement and the successive layers of ABS-15%Al and PA6-50%Al were loosely packed and overlapping of non-mixed layers can be observed. But in the case of joints produced in experiment no. 7 (having maximum mechanical strength with maximum heat generation and minimum forced required), the formation of micrographic structure was very sound with observance of uniformly mixed layers. Hence it can be ascertained that good amount of heat generation with smooth material flow is required to obtain sustainable joints.

Fig. 8 shows macrograph of joints at experiment no. 2 and experiment no. 7. The image at experiment no. 2 highlights the surface with large porosity and non-uniformly stirred zone. It should be noted that lower heat generation at experiment no. 2 resulted into the maximum force requirement that may have further interrupted the layer formation and resulted into porous/ defected surface. Similarly the joint prepared in experiment no. 7 looks more clear, sound with less surface defects as compared to experiment no. 2. This may be because of better heat generation and less force required in experiment no. 7.

4.4. Porosity at joints

The percentage porosity in experiment no. 7 (having maximum heat generation and mechanical sustainability) was observed minimum (14.28%) and in experiment no. 2 (having lowest heat generation and mechanical sustainability) was maximum (24.24%). Hence it is ascertained that high porous joints resulted into less strength (due to the lower heat generation). The force requirements results also indicated

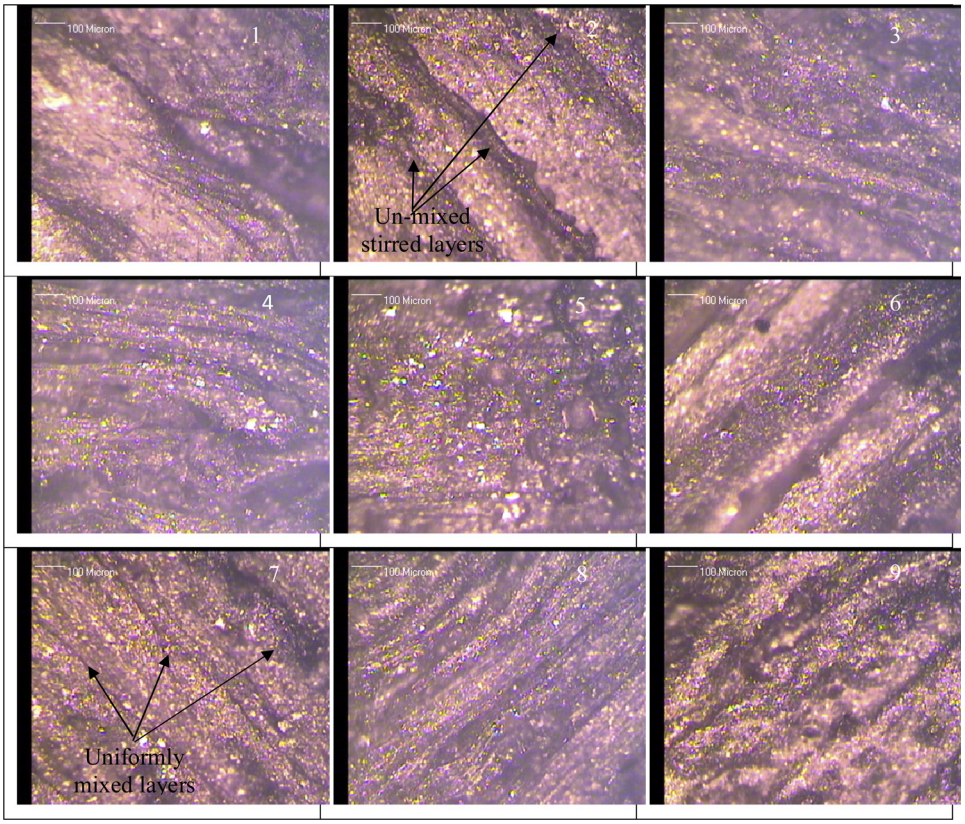

Fig. 7. Photomicrographs of stirred zone (at 100× magnification).

that there would be non-uniformity of stirred surface if heat generation is less. Milling dynamometer compatible with FSW setup moniored the changes in the force requirement during welding process. The maximum axial load was observed in experiment no. 2 (380 N) and minimum force was required for welding in experiment no. 7 (52 N). Finally it may be concluded that experimental conditions in experiment no. 7 are better as stirring exhibited less resistance due to higher rpm, higher plunge depth and low traverse speed.

4.5. DSC interpretation on stirred zone

Since joints have been observed with maximum properties (including heat generation, porosity and force requirements) at experiment no. 7 and minimum at experiment no. 2, the DSC interpretations have been performed on experiment no. 2 and 7 only to check the differences in the thermal properties of those joints in form of melting points, solidification points, integral and normalized heat energy (See Fig. 9). Here the first thermal cycle (heating and cooling: endothermic and exothermic)has been not considered because it is the fact that in the first cycle all the thermal history are associated with main material must be eliminated. The melting point of samples at experiment no. 2 and experiment no. was appeared almost same as 219.60 °C and 219.59 °C, but the integral heat energy was taken more for experiment no. 7 (143.59 mJ) as compared to experiment no. 2 (125.29 mJ). Similarly during solidification, sample at experiment no. 7 (139.12 mJ) released more integral energy as compared to sample at experiment no. 2 (124.75 mJ). Here it is considerable from the thermal studies that more heat generated at experiment no. 7 makes those samples more thermally stable as compared to sample at experiment no. 2.

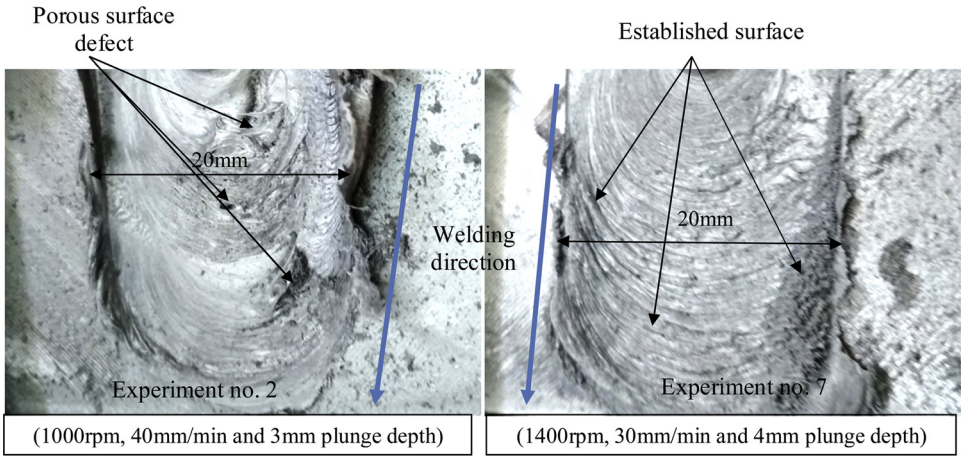

Fig. 8. of joints at different experimental conditions.

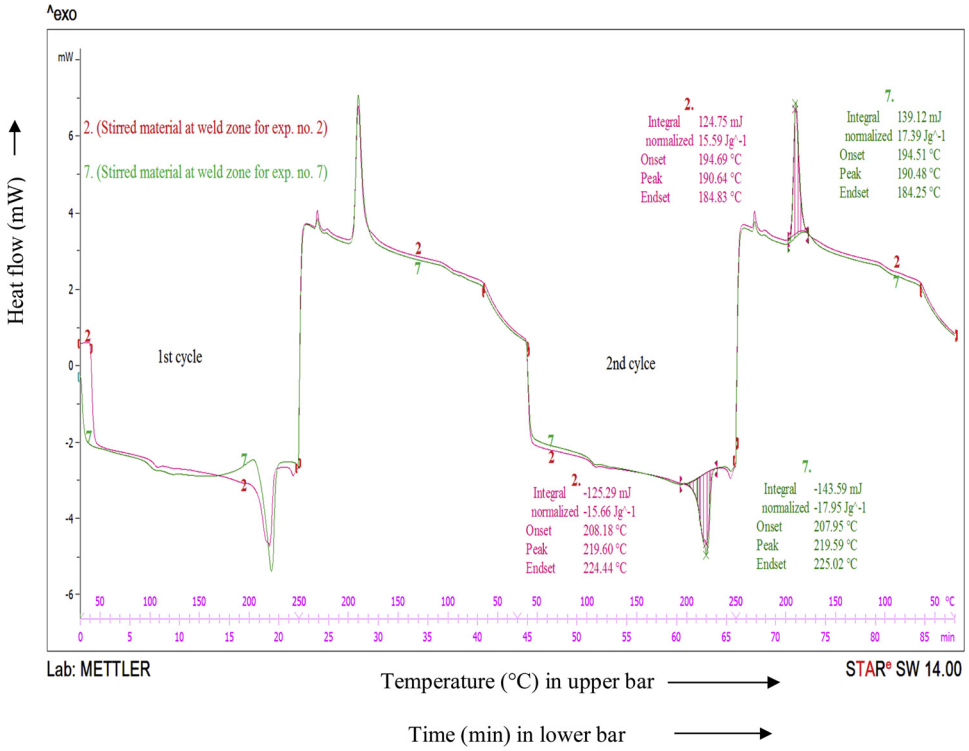

Fig. 9. DSC interpretations for joints at experiment no. 2 and experiment no. 7.

4.6. Factors affecting output parameters

The signal to noise ratio (SNR) for each property has been calculated for investigations of input process variables on joint properties. For mechanical properties such as; tensile and flexural properties is it required always to be maximum the better type case, so for such properties the SN ratio can be calculated as:

$$\eta = -10\log\left[\frac{1}{n}\sum_{k=1}^{n}\frac{1}{y^2}\right]$$

For properties which desired Smaller is better (such as axial force and porosities), SN ratios can be calculated as;

$$\eta = -10\log\left[\frac{1}{n}\sum_{k=1}^{n}y^2\right]$$

Where η is SN ratio, n is the no. of experiment and y is the material properties at experiment no. k. Table 5 shows the SNR for different outputs.

Based upon Table 5, Fig. 10 shows main effect plot for SNR of joint

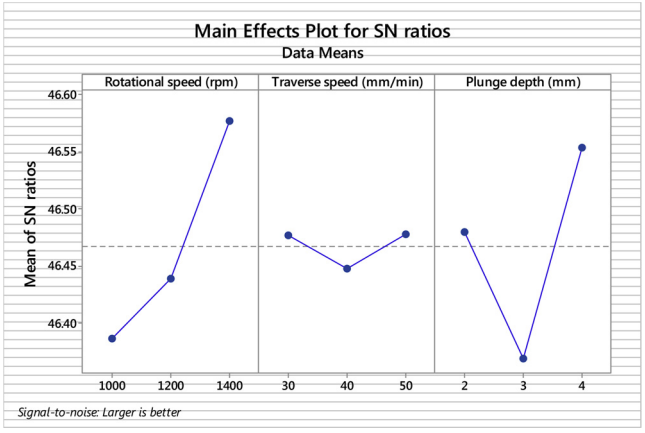

Fig. 10. Main effect plot of SN ration for multi factor optimization.

Table 5
SNR of output parameters.

Exp no.	Tensile properties				Flexural Properties				Axial force	Interface temperature	Porosity at joints
	Peak Load	Break Load	Elongation at Peak	Elongation at Break	Peak Load	Break Load	Deflection at Peak	Deflection at Break			
1	47.34	46.42	6.40	6.40	40.84	40.01	14.20	19.19	−49.57	38.15	−25.68
2	41.48	40.57	−0.44	−0.44	39.16	38.15	−0.44	7.85	−51.59	37.99	−27.69
3	52.31	51.40	7.85	8.49	42.32	41.60	6.40	20.99	−43.04	40.93	−24.32
4	45.58	44.67	1.13	1.13	45.13	44.12	12.80	19.72	−51.12	38.66	−27.01
5	49.81	48.89	9.65	9.65	50.88	49.84	11.59	15.94	−46.06	40.53	−24.70
6	49.54	48.62	5.57	6.40	40.88	40.04	6.40	12.01	−46.84	39.43	−25.14
7	54.46	53.54	11.15	11.15	51.13	50.11	10.18	10.68	−34.32	42.84	−23.21
8	54.14	53.22	10.18	10.18	47.25	46.45	14.82	16.45	−39.64	41.20	−23.97
9	48.24	47.33	10.18	10.18	46.04	45.12	14.82	18.63	−46.44	40.45	−26.09

Table 6
ANOVA for SN ratios.

Input parameters	Degree of freedom	Sequential sum of squares	Adjusted sum of squares	Fisher's value	Probability	Percentage contribution
Rotational speed	2	0.59240	0.592402	23.41	0.041	49.19%
Traverse speed	2	0.00927	0.009267	0.37	0.732	0.76%
Plunge depth	2	0.57725	0.577247	22.81	0.042	47.9%
Residual Error	2	0.02531	0.025311			2.1%
Total	8	1.20423				

properties combined in a single graph from multi factor optimization view point. As observed from Fig. 10, 1400 rpm, 30 mm/min traverse speed and 4 mm plunge depth are the best settings of input parameters from multi factor optimization view point. These results are valid at 95% confidence level. These experimental settings already exists in Table 4 (experimental run 7), which shows already better mechanical properties, so no confirmatory experiment is required.

Further based upon Table 5 analysis of variance (ANOVA) was performed for multifactor optimization view point (see Table 6).

As observed from Table 6 rotational speed followed by plunge depth are most contributing factors with very less error (2.1%). This may be due the fact that rotational speed and plunge depth combination results into more heat generation resulting into better material flow while FSW. These results are in line with the observations made by other investigators [25].

5. Conclusions

a) It has been observed that best tensile and flexural properties were obtained at 1400 rpm, 30 mm/min and 4 mm plunge depth with minimum requirement of force (52 N), whereas worst tensile properties were obtained at 1000 rpm, 40 mm/min and 3 mm plunge depth with maximum force requirement (380 N).
b) Based upon ANOVA (from multifactor optimization view point) it may be concluded that the maximum values of rotational speed followed by plunge depth (available in the present case study) are the most significant parameters (at 95% confidence level) as these parameters helps in better heat generation.
c) It has been observed that porous joints resulted into less strength may be due to the lower heat generation (as because the quality and soundness of the weld is largely dependent upon the temperature/heat generation during stirring). In the present case study force requirements results indicates that there would be non-uniformity of stirred surface if heat generation is compromised. From the thermal studies it has been concluded that more heat was generated in experiment no. 7, which makes those samples more thermally stable as compared to sample in experiment no. 2.

Acknowledgements

The authors are highly thankful to Board of research in nuclear science (BRNS) No: 34/14/10/2016-BRNS/34036 and center for manufacturing research, GNDEC, Ludhiana for providing financial/technical assistance to carry out the research work.

References

[1] Kempers R. Additive manufacturing of continuous wire polymer composites. Manuf Lett 2018;16:49–51.
[2] Garces IT, Ayranci C. A view into additive manufactured electro-active reinforced smart composite structures. Manuf Lett 2018;16:1–5.
[3] Jain R, Pal SK, Singh SB. A study on the variation of forces and temperature in a friction stir welding process: a element approach. J Manuf Process 2016;23:278–86.
[4] Vijendra B, Sharma A. Induction heated tool assisted friction-stir welding (i-FSW): a novel hybrid process for joining of thermoplastics. J Manuf Process 2015;20:234–44.
[5] Sun Z, Wu CS. A numerical model of pin thread effect on material flow and heat generation in shear layer during friction stir welding. J Manuf Process 2018;36:10–21.
[6] Quintana KJ, Silveira JL. Mechanistic models and experimental analysis for the torque in FSW considering the tool geometry and the process velocities. J Manuf Process 2017;30:406–17.
[7] Derazkola HA, Elyasi M. The influence of process parameters in friction stir welding of Al-Mg alloy and polycarbonate. J Manuf Process 2018;35:88–98.
[8] Eslami S, Ramos T, Tavares PJ, Moreira PM. Shoulder design developments for FSW lap joints of dissimilar polymers. J Manuf Process 2015;20:15–23.
[9] Sheikh-Ahmad JY, Ali DS, Deveci S, Almaskari F, Jarrar F. Friction stir welding of high density polyethylene–carbon black composite. J Mater Process Technol 2018;264:402–13.
[10] Kumar R, Singh R, Ahuja IPS. A framework for welding of dissimilar polymers by using metallic fillers. Int J Mater Sci Eng 2017;8(1):101–5.
[11] Kumar R, Singh R, Ahuja IP. Friction stir welding of ABS-15Al sheets by introducing compatible semi-consumable shoulder-less pin of PA6-50Al. Measurement 2019;131:461–72.
[12] Kumar R, Singh R, Ahuja IP. Investigations of mechanical, thermal and morphological properties of FDM fabricated parts for friction welding applications. Measurement 2018;120:11–20.
[13] Singh R, Kumar R, Feo L, Fraternali F. Friction welding of dissimilar plastic/polymer materials with metal powder reinforcement for engineering applications. Compos B Eng 2016;101:77–86.
[14] Kumar R, Singh R, Ahuja IP. Melt processing for enhancing compatibility of aluminum-reinforced acrylonitrile–butadiene–styrene and polyamide 6 for friction welding applications. J Braz Soc Mech Sci Eng 2018;40(8):378.
[15] Azhiri RB, Tekiyeh RM, Zeynali E, Ahmadnia M, Javidpour F. Measurement and evaluation of joint properties in friction stir welding of ABS sheets reinforced by nanosilica addition. Measurement 2018;127:198–204.
[16] Baffari D, Buffa G, Campanella D, Valvo EL, Fratini L. Experimental and numerical investigation on a new FSW based metal to composite joining technique. J Manuf Process 2018;34:758–64.
[17] Banjare PN, Sahlot P, Arora A. An assisted heating tool design for FSW of thermoplastics. J Mater Process Technol 2017;239:83–91.
[18] Evans WT, Gibson BT, Reynolds JT, Strauss AM, Cook GE. Friction stir Extrusion: a new process for joining dissimilar materials. Manuf Lett 2015;5:25–8.
[19] Huang Y, Meng X, Wang Y, Xie Y, Zhou L. Joining of aluminum alloy and polymer via friction stir lap welding. J Mater Process Technol 2018;257:148–54.
[20] Huang Y, Meng X, Xie Y, Wan L, Lv Z, Cao J, et al. Friction stir welding/processing of polymers and polymer matrix composites. Compos A Appl Sci Manuf 2017;105:235–57.
[21] Huang Y, Meng X, Xie Y, Li J, Wan L. Joining of carbon fiber reinforced thermoplastic and metal via friction stir welding with co-controlling shape and performance. Compos A Appl Sci Manuf 2018. https://doi.org/10.1016/j.compositesa.2018.06.027.
[22] Padhy GK, Wu CS, Gao S. Friction stir based welding and processing technologies-processes, parameters, microstructures and applications: a review. J Mater Sci Technol 2018;34(1):1–38.
[23] Singh R, Kumar R, Ahuja IP. Mechanical, thermal and melt flow of aluminum-reinforced PA6/ABS blend feedstock filament for fused deposition modeling. Rapid Prototyp J 2018. https://doi.org/10.1108/RPJ-05-2017-0094.
[24] Kumar R, Singh R, Ahuja IP, Amendola A, Penna R. Friction welding for the manufacturing of PA6 and ABS structures reinforced with Fe particles. Compos B Eng 2018;132:244–57.
[25] Lambiase F, Paoletti A, Grossi V, Di Ilio A. Analysis of loads, temperatures and welds morphology in FSW of polycarbonate. J Mater Process Technol 2018;266:639–50.
[26] Lambiase F, Genna S. Laser-assisted direct joining of AISI304 stainless steel with polycarbonate sheets: thermal analysis, mechanical characterization, and bonds morphology. Opt Laser Technol 2017;88:205–14.
[27] Lambiase F, Paoletti A, Di Ilio A. Forces and temperature variation during friction stir welding of aluminum alloy AA6082-T6. Int J Adv Manuf Technol 2018;99(1-4):337–46.
[28] Okada T, Ishige R, Ando S. Analysis of thermal radiation properties of polyimide and polymeric materials based on atr-ir spectroscopy. J Photopolym Sci Technol 2016;29(2):251–4.
[29] https://permalink.lanl.gov/object/tr?what=info:lanl-repo/lareport/LA-UR-17-20513, retrieved on Dec 18 2018.
[30] https://www.engineeringtoolbox.com/radiation-heat-emissivity-aluminum-d_433.html, retrieved on Dec 18 2018.